Widespread inhibitory responses in the mouse olfactory sensory neurons *in vivo*

Shigenori Inagaki[1,4], Ryo Iwata[2,4], and Takeshi Imai[1,2,3,4,5,*]

Affiliations:

[1] Graduate School of Medical Sciences, Kyushu University, Fukuoka 812-8582, Japan.

[2] Laboratory for Sensory Circuit Formation, RIKEN Center for Developmental Biology, Kobe 650-0047, Japan.

[3] Research and Development Center for Five-Sense Devices, Kyushu University, Fukuoka 819-0395, Japan.

[4] Contributed equally

[5] Lead Contact

*Correspondence: t-imai@med.kyushu-u.ac.jp

SUMMARY

Odor recognition starts from olfactory sensory neurons (OSNs), but this process is yet to be fully understood in physiological conditions *in vivo*. Here, we performed two-photon calcium imaging of mouse olfactory sensory neurons *in vivo* and found that odors produce not only excitatory, but also inhibitory responses at their axon terminals. Robust inhibitory responses at OSN axon terminals remained in two independent mutant mice, in which all possible sources of presynaptic lateral inhibition were eliminated. Therefore, we examined the responses in the olfactory epithelium *in vivo*, and found robust and widespread inhibitory responses at the level of OSN somata. Moreover, responses to odor mixtures demonstrated extensive mutual modulation (both suppression and enhancement) in OSNs. An *in vitro* assay demonstrated that some odorants act as inverse agonists to some odorant receptors. The bidirectional nature of OSN responses may be useful for robust odor coding under noisy sensory environment.

INTRODUCTION

Sensory systems have to detect biologically meaningful sensory signals from noisy background signals. For example, the visual system has to detect a visual cue in the presence of background signals and under ambient light. In order to detect specific visual features, both decreases and increases in neurotransmission from photoreceptor cells are conveyed to the ON and OFF pathways, respectively. In addition, lateral inhibition in the retina enables the contrast enhancement of spatial information, thus aiding the detection of a visual object (Demb and Singer, 2015). The key features of the visual system are the bidirectional nature of the photoreceptor cell responses to visual objects, which are both excitatory and inhibitory.

Similarly, the olfactory system has to reliably detect fluctuating odor molecules under various background signals. In fact, natural environments often contain a lot of ambient odorants. In addition, accumulating evidence shows that many OSNs robustly respond to mechanical stimuli produced by the nasal airflow (Chen et al., 2012; Connelly et al., 2015; Grosmaitre et al., 2007; Iwata et al., 2017). As a result, sniffing alone produces responses in many OSNs without odors. Moreover, animals can identify an odor from temporally dynamic odor plume. How specific odor information is reliably extracted from such noisy signals in physiological conditions is a central issue in the field. The olfactory bulb (OB) and cortical circuits certainly play important roles for this task (Imai, 2014; Wilson and Mainen, 2006). In particular, the roles of inhibitory circuits have been well recognized, in terms of gain control, lateral inhibition, and temporal patterning (Banerjee et al., 2015; Economo et al., 2016; Fukunaga et al., 2014; Kato et al., 2013; McGann et al., 2005; Yokoi et al., 1995). However, we know little about odor information processing at the entry point of the olfactory system, the OSNs, in the physiological context *in vivo*.

In the mammalian olfactory system, each OSN expresses just one type of odorant receptor (OR) out of a large repertoire (~1000 in mice), and OSNs expressing the same type of OR converge their axons to a common glomerulus in the OB. It is also known that all types of ORs in the main olfactory system couple to G_{olf}, and cAMP signals regulate depolarization of OSNs via CNG channels (Firestein, 2001). So far, most electrophysiological or calcium imaging studies of OSN somata have been limited to isolated OSNs or olfactory epithelium (OE). Due to the limited throughput of these methodologies, it has been difficult to obtain comprehensive odor response profiles at the level of OSNs. Imaging of the OB, based on intrinsic signals (Rubin and Katz, 1999), chemical calcium dyes (Wachowiak and Cohen, 2001), and synapto-pHluorin (Bozza et al., 2004), has been powerful in our understanding of the odor coding based on the glomerular map. However, the sensitivity and temporal resolution have been limited in these studies. While more sensitive GCaMP sensors are commonly used for calcium imaging of OB neurons (Wachowiak et al., 2013), its use for OSNs has been limited (Iwata et al., 2017). Based on our limited knowledge, it has been generally believed that odorants “activate” OSNs, and odor information is represented by the map of “activated” glomeruli in the OB.

Here we performed GCaMP calcium imaging of OSNs and found widespread inhibitory responses at OSN axon terminals in the OB. We also found that inhibitory responses are already evident at the OSN somata showing inverse agomism. Moreover, a response to an odor mixture demonstrated extensive suppression and a non-linear enhancement. Thus, both excitatory and inhibitory responses in the OSNs themselves contribute to the odor coding in the mammalian olfactory system.

RESULTS

Inhibitory responses at OSN axon terminals *in vivo*

In order to understand the odor information processing in the mammalian olfactory system, it is fundamental to understand the odor responses at the most peripheral level, the OSNs. Previously, calcium imaging of OSNs has been performed through cranial windows over the OB. In these studies, chemical dyes (e.g., calcium green-1) were loaded to OSNs through the OE; however, this loading method was inefficient, and the maximum response amplitude was only up to ~10% $\Delta F/F_0$ in typical experiments (Wachowiak and Cohen, 2001). A fluorescent indicator for synaptic vesicle release, synapto-pHluorin (spH), was a much more sensitive sensor for OSN activity (Bozza et al., 2004); however, its temporal resolution was much slower than calcium indicators, which hampered studies of dynamic responses.

In this study, we used an OSN-specific GCaMP transgenic mice, OSN-GCaMP3 (*OMP-tTA; TRE-GCaMP3* compound heterozygous BAC transgenic mice, Figure 1A), as described in a previous study (Iwata et al., 2017). When the OB was imaged with two-photon microscopy, we could obtain highly reliable response signals (up to ~200% $\Delta F/F_0$) for various odorants (amyl acetate, heptanal, valeraldehyde, and cyclohexanone, diluted at 0.5%). Unexpectedly, we often observed reductions in GCaMP signals (up to ~20% $\Delta F/F_0$ reduction) upon odor stimulation (Figure 1B, C, S1). This is most likely due to the suppression of spontaneous activity as has been seen in mitral/tufted (M/T) cell imaging (Economo et al., 2016), thus representing inhibitory responses. The inhibitory responses were shared across fibers within a glomerulus, suggesting that the inhibition is OR-specific, rather than random (Figure 1B). It should be noted that the inhibitory responses would be only seen, in theory, for OSNs with high spontaneous activity. These inhibitory responses have been overlooked in previous studies, most likely due to the low sensitivity and/or slower kinetics of the sensors.

We measured responses to four pure odorants (amyl acetate, heptanal, valeraldehyde, and cyclohexanone, diluted at 0.5%) for 299 glomeruli (5 mice in total) and inhibitory responses were commonly observed for all the four odorants (Figure 1D, E; data for more odorants are described in Figure S1). These responses were reproducible across 3 trials (Figure S1B). Similarly to the excitatory responses, the inhibitory responses were broadly tuned in some, but narrowly tuned in other glomeruli (Figure 1F). In this dataset, 56% and 12% of glomeruli demonstrated excitatory and inhibitory responses, respectively (defined for >3 standard deviations (SD) changes). A substantial fraction of glomeruli demonstrated binary responses, showing excitation to some and inhibition to other odorants (e/i fraction in Figure 1D). The temporal kinetics was different between excitatory and inhibitory responses. In general, inhibitory responses were slower, showing response peaks at 5-25 sec after odor stimulation (Figure S1A, C). Some glomeruli demonstrated more complex bi-phasic responses, showing excitatory-inhibitory or inhibitory-excitatory responses (Figure 1C, S1B). While most of our experiments were performed under anesthesia, we also observed inhibitory responses in OSN axons in awake animals (Figure S1D, E).

It has been known that ~50% of OSNs show mechanosensory responses (Grosmaitre et

al., 2007; Iwata et al., 2017). In the *in vivo* situation, sniffing alone can produce airflow-dependent mechanical responses in OSNs. Using artificial sniffing, we have examined the responses to changes in the nasal airflow speed. Again in this experiment, we observed both excitatory and inhibitory responses to increased airflow in OSN axon terminals (Figure S2).

Inhibitory responses at OSN axon terminals remained without presynaptic inhibition

Next we investigated the origin of the inhibitory responses seen at OSN axon terminals. The inhibitory responses to odors may be derived from presynaptic lateral inhibition within the OB circuit. Like photoreceptor cells in the retina, OSN axons receive presynaptic inhibition from OB interneurons. A previous study using spH mice and pharmacology indicated that presynaptic inhibition occurs only within a glomerulus, and lateral presynaptic inhibition plays little or no role in odor responses (McGann et al., 2005). However, another study suggested a role for presynaptic lateral inhibition (Fleischmann et al., 2008). A subset of juxtaglomerular interneurons in the OB (dopaminergic and GABAergic short axon cells) are known to innervate multiple glomeruli, and thus may be a potential source for interglomerular lateral inhibition (Kosaka and Kosaka, 2008). We therefore examined whether interglomerular presynaptic inhibition could play a role by using conditional mutant mice.

It has been known that GABA and dopamine play major roles in the presynaptic inhibition of OSN axon terminals (Aroniadou-Anderjaska et al., 2000; Ennis et al., 2001; McGann et al., 2005). GABA-dependent presynaptic inhibition is mediated by the $GABA_B$ receptor. A functional $GABA_B$ receptor is a heterodimer consisting of $GABA_{B1}$ and $GABA_{B2}$ subunits (Bettler et al., 2004). We therefore generated a conditional mutant mouse line for $GABA_{B1}$, which constitutes a GABA-binding subunit. As for dopamine, the D2 receptor is known to mediate presynaptic inhibition (Ennis et al., 2001). We therefore generated a conditional mutant mouse line for D2R (see Figure S3 and Methods for details). Immunostaining of OB sections from the conditional mutant mice show a much reduced expression of $GABA_B$ receptors and D2R. The weak remaining signals are most likely derived from OB neurons (Figure S3). Crossed with the *OMP-Cre* knock-in line, we generated an OSN-specific double knockout animals for both $GABA_{B1}$ and D2R (Figure 2A; *OMP-Cre; Gabbr1*$^{fl/fl}$*; D2R*$^{fl/fl}$). We examined odor responses using OSN-GCaMP (i.e., *OMP-tTA; TRE-GCaMP3; OMP-Cre; Gabbr1*$^{fl/fl}$*; D2R*$^{fl/fl}$ mice). However, we still observed both excitatory and inhibitory responses at OSN axon terminals (Figure 2B). The amplitudes and the temporal kinetics of excitatory and inhibitory responses were only slightly different from the wild-type mice (Figure 2D).

Although GABA and dopamine have been considered to play major roles in presynaptic inhibition in OSN axons, we cannot rule out the contribution of unknown types of presynaptic inhibition mediated by the OB neurons. We therefore generated OSN-specific tetanus toxin light chain (TeNT) knock-in mice, in which synaptic transmission from OSNs is blocked (Figure 2A, *OMP-Cre; R26-CAG-loxP-TeNT*, OSN-TeNT hereafter)(Sakamoto et al., 2014)(Fujimoto et al.,

2019). Using an M/T cell-specific GCaMP6f mouse line (Dana et al., 2014; Iwata et al., 2017), we confirmed that the odor responses in M/T cells are almost completely shut off in OSN-TeNT mice (Figure S4). Because neurotransmission from OSNs is abolished, all kinds of presynaptic inhibition from OB neurons should be eliminated in this mouse line. Nevertheless, a substantial fraction of glomeruli still demonstrated inhibitory responses to odor stimuli in OSN axon terminals (Figure 2).

It is possible that homeostatic plasticity has masked some aspects of presynaptic inhibition under the chronic inactivation present in these mutant mice. Therefore, presynaptic inhibition may partly contribute to the inhibitory responses seen at OSN axons. However, results so far strongly suggest that a substantial fraction of inhibitory responses is generated within OSNs, without any contribution from OB interneurons.

Inhibitory responses at OSN somata in the OE

A straightforward way to confirm this possibility is to record odor responses in the OSN somata in the OE *in vivo*. We have recently established *in vivo* two-photon imaging of OSN somata in the OE (Figure 3A)(Iwata et al., 2017). In our OSN-GCaMP3 mice, only a subset of OSNs (~60%) expresses GCaMP3, allowing for the separation of most of somatic signals. In addition, due to the high basal fluorescence of GCaMP3 (Figure 3B), we were able to record all kinds of odor responses. We examined the odor responses of OSN somata and found that the inhibitory responses are also widespread in the OE (Figure 3C, D). Using the same sets of odorants as used for the OSN axon imaging, we found that 5% of OSN responses are inhibitory at the somata (defined for >3SD changes) (Figure 3E, F). Inhibitory responses at OSN somata were more narrowly tuned than in OSN axon terminals (Figure 3G). However, as the fluorescence signals are much weaker than in the glomeruli, it is difficult to compare them quantitatively.

Representation of odor mixtures in OSNs

The inhibition would have more impact on the representation of odor mixtures, as has been well known in M/T cells (Economo et al., 2016; Yokoi et al., 1995). Although earlier studies focused on lateral inhibition within the OB circuit, we considered that odor mixture may be more dynamically represented at the OSN level than has considered previously. Here we examined the OSN axon responses for amyl acetate, valeraldehyde, and a mixture of amyl acetate + valeraldehyde. We often observed that one odorant reduces or abolishes the responses to the other odorant at various degrees (Figure 4A-D). We obtained similar results for various odor mixtures (Figure S6A-C). The suppressive effects of the odor mixture representation were seen not only for glomeruli demonstrating inhibitory-excitatory responses to the odor pair, but also for null-excitatory and even for some excitatory-excitatory cases (Figure 4E, G). When we analyzed glomeruli showing excitatory responses to an odorant (odor 2) and excitatory or null responses to another (odor 1), 58% of glomeruli demonstrated suppression by odor 1(Figure 4E, G). These suppressed responses were also seen in OSN-specific $GABA_{B1}$/D2R double knockout mice (data

not shown).

A more puzzling observation was the non-linear enhancement of odor responses in the odor mixture experiment. For example, the responses to a mixture of amyl acetate + valeraldehyde were much greater than the linear sum of amylacetate and valeraldehyde responses in some glomeruli (Figure 4B, glomerulus #2). Here we only focused on glomeruli showing excitatory responses to an odorant (odor 2) and null or inhibitory responses to another (odor 1), but 17% of cases demonstrated enhanced responses over the response to odor 2 (Figure 4F, G).

OSN somata also demonstrated similar suppression and enhancer effects by using odor mixtures (Figure 5A-D, S6D-F). When we only analyzed OSN somata showing excitatory responses to an odorant (odor 2) and excitatory or null responses to another (odor 1), 13% of them demonstrated suppression by odor 1 (Figure 5E, G). When we analyzed OSN somata that showed excitatory responses to an odorant (odor 2) and null or inhibitory responses to another (odor 1), 18% of them demonstrated enhancement by odor 1 (Figure 5F, G).

Taken together, the results indicate that, the responses to the odor mixture are extensively modulated (either suppressed or enhanced), and are not always the linear sum of the individual ones.

Odorants act as inverse agonists for some ORs in heterologous assay system

What are the origins of the inhibitory responses seen in OSN somata? In one scenario, the inhibitory responses may be a result of non-synaptic lateral inhibition known as ephaptic coupling. In the *Drosophila* olfactory system, 2-3 OSNs are tightly packed within a sensillum, and electrically affect to each other (Su et al., 2012; Zhang et al., 2019). This may occur within the tightly packed OE and axon bundles in mice (Bokil et al., 2001); however, as each type of OSN is randomly scattered in the OE, so ephaptic coupling alone cannot account for the OR-specific inhibitory responses found at axon terminals (Figure 1B). We therefore considered the possibility that the inhibitory responses occurs at the OR level, as has also been proposed for *Drosophila* OSNs (Cao et al., 2017; Hallem et al., 2004). Although receptor antagonism has been well known (Araneda et al., 2004; Kurahashi et al., 1994; Oka et al., 2004; Rospars et al., 2008; Tsuboi et al., 2011), inhibitory responses are not fully established for mammalian ORs.

To study the inhibitory responses at the receptor level, we used a heterologous assay system. ORs were co-expressed with a chaperone molecule, RTP1S, in HEK293 cells. We examined cAMP responses based on cAMP-response element (CRE) promoter activity using a dual luciferase assay system (See Methods for details) (Saito et al., 2004; Tsuboi et al., 2011). In the initial screen, we expressed 83 mouse ORs, and measured the basal activity without odorants. We then focused on the 11 ORs with the highest basal activity, as it would be easier to find inhibitory responses for these ORs. We then examined the responses of these ORs to 9 odorants. We found that Olfr644 (also known as MOR13-1) and Olfr1054 (MOR188-2) show inhibitory responses to odorants. For Olfr644, benzaldehyde acted as an agonist, but heptanal and amyl

acetate were inverse agonists showing receptor inhibition (Figure 6A). Similarly for Olfr1054, acetophenone was an agonist, but ethylhexanoate was an inverse agonist (Figure 6B). Thus, the inhibitory responses occur, at least in part, at the receptor level.

DISCUSSION

It has long been considered that odorants activate ORs, and OSNs send excitatory inputs to the OB. However, our *in vivo* imaging study demonstrated that odorants elicit not only excitatory, but also inhibitory responses in OSNs, thus revising the classical view. These inhibitory responses are widespread phenomena in the mammalian OSNs.

What are the origins of the inhibitory responses in OSNs? In the mammalian retina, horizontal cells are known to mediate lateral inhibition, and the inhibition by horizontal cells occurs both presynaptically on photoreceptor cells, and postsynaptically on bipolar cells (Demb and Singer, 2015). We therefore considered a possible contribution of presynaptic lateral inhibition by OB interneurons. However, two independent mutant mice lacking known types of presynaptic inhibition still demonstrated inhibitory responses at OSN axon terminals. Moreover, we found that inhibitory responses already exist at the level of OSN somata. These results suggest that a substantial fraction of inhibitory responses originate from the OE. However, as there are some differences between OSN somata and axon terminals (e.g., tuning specificity and degree of mixture effects), it is likely that there is also a contribution from interglomerular presynaptic inhibition by the OB interneurons (Fleischmann et al., 2008).

In the *Drosophila* olfactory system, it has been reported that ephaptic coupling within sensilla and inverse agonism contribute to the inhibitory responses at the OSN somata (Hallem et al., 2004; Su et al., 2012). As OSNs and their axons are tightly packed, ephaptic coupling may also occur in the mammalian olfactory system (Bokil et al., 2001). However, given the random distribution of OSNs in the OE, this does not seem to account for the OR-specific inhibitory responses seen in OSN axon terminals (Figure 1). Using a reconstituted system, we showed that odorants act as inverse agonists at least for some ORs (Figure 6), consistent with a previous report on OSN electrophysiology (Reisert, 2010). It has been known that the basal activity of ORs is important for OSN development: Many of the ORs have basal activity without odorants and the basal cAMP level contributes to axonal wiring specificity during development (Imai and Sakano, 2008; Imai et al., 2006; Imai et al., 2009; Nakashima et al., 2013). While basal activity has been reported using the electrophysiological recording of isolated mature OSNs (Reisert, 2010), its role in odor coding has been unknown. Our current study suggests that the basal activity of mature OSNs contributes to bidirectional responses, excitatory and inhibitory, to odorants. It is possible that OSNs with high basal activity tend to show inhibitory responses to various odorants (Figure 3E, G), as has been shown for M/T cells in awake animals (Kollo et al., 2014).

In addition to inverse agonism, it is also possible that antagonism has contributed to the apparent inhibitory responses seen in our *in vivo* study. OSNs may respond to ambient odors as

well as metabolites in the olfactory mucosa in the physiological condition *in vivo*. In addition, the OSNs respond to mechanical stimuli produced by the nasal airflow. Although the exact mechanism is yet to be established, an *in vitro* study suggested that ORs may directly recognize mechanical stimuli, similarly to odor recognition (Connelly et al., 2015). Therefore, antagonistic odorants can suppress these responses. In the visual system, opsin proteins themselves have extremely low basal activity; however, the ambient light allows for bidirectional responses (inhibition and excitation) in photoreceptor cells that are conveyed to ON/OFF pathways, respectively (Figure 6D). Similarly, hair cells in the auditory and vestibular systems are known to show bidirectional responses. The inhibitory responses in OSNs may be useful for robust odor identification under noisy sensory environment (Figure 6D).

Antagonism for ORs has been studied with various ORs, including rat I7, MOR-EG, and MOR29B (Araneda et al., 2004; Oka et al., 2004; Tsuboi et al., 2011). However, it has yet to be fully established how the OR antagonism impact olfaction *in vivo*. In the current study we showed that the responses to odor mixtures are already extensively modulated at the peripheral level *in vivo*. Responses to an odorant are inhibited by another in >50% of glomeruli and >10% of OSN somata, supporting the idea that the extensive antagonism tunes the representation of odor mixtures in OSNs (Figure 5). Our *in vivo* observations are in good agreement with recent studies using *ex vivo* imaging and reconstituted systems. Unexpectedly, a substantial fraction of OSNs (10-20% both in glomeruli and OSN somata) demonstrated enhanced odor responses when mixed together (Figure 4 and 5). Although enhanced responses at axons may be partly due to the dis-inhibition of OB inhibitory circuits, we could still see the enhanced responses at OSN somata. This may be due to the allosteric enhancer effect of an odorant to another, as has been known to occur for various GPCRs including taste receptors (Schwartz and Holst, 2007). This issue needs to be addressed in future studies *in vitro*. Together, our results revise a prevailing view in which odor mixtures are represented as a linear sum of individual ones in OSNs (Lin et al., 2006). Previous studies proposed that non-linear representation of odor mixtures occurs in the olfactory cortex (Stettler and Axel, 2009), but this is in fact happening already in OSNs.

In the OB, it has been well known that M/T cell responses are highly dynamic, particularly in awake conditions. M/T cells show both excitatory and inhibitory responses, contributing to timing-based representation of odor information (Cury and Uchida, 2010; Economo et al., 2016; Iwata et al., 2017; Kollo et al., 2014; Shusterman et al., 2011). Therefore, both excitatory and inhibitory responses in OSNs should contribute to the odor coding in the OB. We propose that extensive inhibition and modulation at the receptor level contribute to the odor coding in the mammalian olfactory system (Figure 6D).

ACKNOWLEDGMENTS

We thank KOMP and EUCOMM for ES clones (conditional *Drd2* and *Gabbr1*); M. Yokoi (*Pcdh21-Cre*), I. Imayoshi (*R26-CAG-LoxP-TeNT*), K. Svoboda (*Thy1-GCaMP6f*), and P. Mombaerts (*OMP-Cre* knock-in) for mouse strains; Marcus Leiwe for comments on the

manuscript. Animal experiments including generation of chimeric mice were supported by the Laboratory for Animal Resources and Genetic Engineering at the RIKEN Center for Life Science Technologies. We appreciate the technical assistance by Mariko Nishihara, Masakazu Iwamoto, and from The Research Support Center, Research Center for Human Disease Modeling, Kyushu University Graduate School of Medical Sciences. This work was supported by grants from the PRESTO program of the Japan Science and Technology Agency (JST) (T.I.), the JSPS KAKENHI (23680038, 15H05572, 15K14336, 16K14568, 16H06456, and 17H06261 to T.I., 15K18353 to R.I.), intramural grant from RIKEN Center for Developmental Biology (T.I.), and Grant-in-Aid for JSPS Research Fellow (15J08987 to R.I., and 18J00899 to S.I.).

AUTHOR CONTRIBUTIONS

S.I. performed experiments and analyzed data. R.I. generated knockout and transgenic mice, and performed initial rounds of imaging experiments. T.I. supervised the project. S.I. and T.I. wrote the manuscript.

REFERENCES

Araneda, R.C., Peterlin, Z., Zhang, X., Chesler, A., and Firestein, S. (2004). A pharmacological profile of the aldehyde receptor repertoire in rat olfactory epithelium. Journal of Physiology-London *555*, 743-756.

Aroniadou-Anderjaska, V., Zhou, F.M., Priest, C.A., Ennis, M., and Shipley, M.T. (2000). Tonic and synaptically evoked presynaptic inhibition of sensory input to the rat olfactory bulb via GABA(B) heteroreceptors. J Neurophysiol *84*, 1194-1203.

Banerjee, A., Marbach, F., Anselmi, F., Koh, M.S., Davis, M.B., da Silva, P.G., Delevich, K., Oyibo, H.K., Gupta, P., Li, B., *et al.* (2015). An Interglomerular Circuit Gates Glomerular Output and Implements Gain Control in the Mouse Olfactory Bulb. Neuron *87*, 193-207.

Bettler, B., Kaupmann, K., Mosbacher, J., and Gassmann, M. (2004). Molecular structure and physiological functions of GABA(B) receptors. Physiological Reviews *84*, 835-867.

Bokil, H., Laaris, N., Blinder, K., Ennis, M., and Keller, A. (2001). Ephaptic interactions in the mammalian olfactory system. Journal of neuroscience *21*, RC173.

Bozza, T., McGann, J.P., Mombaerts, P., and Wachowiak, M. (2004). In vivo imaging of neuronal activity - Neurotechnique by targeted expression of a genetically encoded probe in the mouse. Neuron *42*, 9-21.

Cao, L.H., Yang, D., Wu, W., Zeng, X.K., Jing, B.Y., Li, M.T., Qin, S.S., Tang, C., Tu, Y.H., and Luo, D.G. (2017). Odor-evoked inhibition of olfactory sensory neurons drives olfactory perception in Drosophila. Nature Communications *8*.

Chen, X.M., Xia, Z.G., and Storm, D.R. (2012). Stimulation of Electro-Olfactogram Responses in the Main Olfactory Epithelia by Airflow Depends on the Type 3 Adenylyl Cyclase. Journal of Neuroscience *32*, 15769-15778.

Connelly, T., Yu, Y.Q., Grosmaitre, X., Wang, J., Santarelli, L.C., Savigner, A., Qiao, X., Wang, Z.S., Storm, D.R., and Ma, M.H. (2015). G protein-coupled odorant receptors underlie mechanosensitivity in mammalian olfactory sensory neurons. Proceedings of the National Academy of Sciences of the United States of America *112*, 590-595.

Cury, K.M., and Uchida, N. (2010). Robust odor coding via inhalation-coupled transient activity in the mammalian olfactory bulb. Neuron *68*, 570-585.

Dana, H., Chen, T.W., Hu, A., Shields, B.C., Guo, C.Y., Looger, L.L., Kim, D.S., and Svoboda, K. (2014). Thy1-GCaMP6 Transgenic Mice for Neuronal Population In Vivo. PLoS One *9*.

Demb, J.B., and Singer, J.H. (2015). Functional Circuitry of the Retina. Annu Rev Vis Sci *1*, 263-289.

Economo, M.N., Hansen, K.R., and Wachowiak, M. (2016). Control of Mitral/Tufted Cell Output by Selective Inhibition among Olfactory Bulb Glomeruli. Neuron *91*, 397-411.

Ennis, M., Zhou, F.M., Ciombor, K.J., Aroniadou-Anderjaska, V., Hayar, A., Borrelli, E., Zimmer, L.A., Margolis, F., and Shipley, M.T. (2001). Dopamine d2 receptor-mediated presynaptic inhibition of olfactory nerve terminals. J Neurophysiol *86*, 2986-2997.

Firestein, S. (2001). How the olfactory system makes sense of scents. Nature *413*, 211-218.

Fleischmann, A., Shykind, B.M., Sosulski, D.L., Franks, K.M., Glinka, M.E., Mei, D.F., Sun, Y.H., Kirkland, J., Mendelsohn, M., Albers, M.W., *et al.* (2008). Mice with a "Monoclonal Nose": Perturbations in an Olfactory Map Impair Odor Discrimination. Neuron *60*, 1068-1081.

Fujimoto, S., Leiwe, M.N., Sakaguchi, R., Muroyama, Y., Kobayakawa, R., Kobayakawa, K., Saito, T., and Imai, T. (2019). Spontaneous activity generated within the olfactory bulb establishes the discrete wiring of mitral cell dendrites. bioRxiv, 625616.

Fukunaga, I., Herb, J.T., Kollo, M., Boyden, E.S., and Schaefer, A.T. (2014). Independent control of gamma and theta activity by distinct interneuron networks in the olfactory bulb. Nature Neuroscience *17*, 1208-1216.

Grosmaitre, X., Santarelli, L.C., Tan, J., Luo, M., and Ma, M. (2007). Dual functions of mammalian olfactory sensory neurons as odor detectors and mechanical sensors. Nature neuroscience *10*, 348-354.

Guo, Z.C.V., Hires, S.A., Li, N., O'Connor, D.H., Komiyama, T., Ophir, E., Huber, D., Bonardi, C., Morandell, K., Gutnisky, D., *et al.* (2014). Procedures for Behavioral Experiments in Head-Fixed Mice. PLoS One *9*.

Hallem, E.A., Ho, M.G., and Carlson, J.R. (2004). The molecular basis of odor coding in the drosophila antenna. Cell *117*, 965-979.

Imai, T. (2014). Construction of functional neuronal circuitry in the olfactory bulb. Semin Cell Dev Biol *35*, 180-188.

Imai, T., and Sakano, H. (2008). Odorant receptor-mediated signaling in the mouse. Current Opinion in Neurobiology *18*, 251-260.

Imai, T., Suzuki, M., and Sakano, H. (2006). Odorant receptor-derived cAMP signals direct axonal targeting. Science *314*, 657-661.

Imai, T., Yamazaki, T., Kobayakawa, R., Kobayakawa, K., Abe, T., Suzuki, M., and Sakano, H. (2009). Pre-Target Axon Sorting Establishes the Neural Map Topography. Science *325*, 585-590.

Iwata, R., Kiyonari, H., and Imai, T. (2017). Mechanosensory-Based Phase Coding of Odor Identity in the Olfactory Bulb. Neuron *96*, 1139-+.

Kato, H.K., Gillet, S.N., Peters, A.J., Isaacson, J.S., and Komiyama, T. (2013). Parvalbumin-expressing interneurons linearly control olfactory bulb output. Neuron *80*, 1218-1231.

Kollo, M., Schmaltz, A., Abdelhamid, M., Fukunaga, I., and Schaefer, A.T. (2014). 'Silent' mitral cells dominate odor responses in the olfactory bulb of awake mice. Nature Neuroscience *17*, 1313-1315.

Kosaka, T., and Kosaka, K. (2008). Tyrosine hydroxylase-positive GABAergic juxtaglomerular neurons are the main source of the interglomerular connections in the mouse main olfactory bulb. Neurosci Res *60*, 349-354.

Kurahashi, T., Lowe, G., and Gold, G.H. (1994). Suppression of Odorant Responses by Odorants in Olfactory Receptor-Cells. Science *265*, 118-120.

Li, J.S., Ishii, T., Feinstein, P., and Mombaerts, P. (2004). Odorant receptor gene choice is reset by nuclear transfer from mouse olfactory sensory neurons. Nature *428*, 393-399.

Lin, D.Y., Shea, S.D., and Katz, L.C. (2006). Representation of natural stimuli in the rodent main olfactory bulb. Neuron *50*, 937-949.

McGann, J.P., Pirez, N., Gainey, M.A., Muratore, C., Elias, A.S., and Wachowiak, M. (2005). Odorant representations are modulated by intra- but not interglomerular presynaptic inhibition of olfactory sensory neurons. Neuron *48*, 1039-1053.

Nakashima, A., Takeuchi, H., Imai, T., Saito, H., Kiyonari, H., Abe, T., Chen, M., Weinstein, L.S., Yu, C.R., Storm, D.R., *et al.* (2013). Agonist-Independent GPCR Activity Regulates Anterior-Posterior Targeting of Olfactory Sensory Neurons. Cell *154*, 1314-1325.

Oka, Y., Omura, M., Kataoka, H., and Touhara, K. (2004). Olfactory receptor antagonism between odorants. Embo Journal *23*, 120-126.

Pfister, P., Smith, B.C., Evans, B.J., Brann, J.H., Trimmer, C., Sheikh, M., Arroyave, R., Reddy, G., Jeong, H.-Y., Raps, D.A., *et al.* (2019). Odorant Receptor Inhibition is Fundamental to Odor Encoding. bioRxiv, 760033.

Reisert, J. (2010). Origin of basal activity in mammalian olfactory receptor neurons. J Gen Physiol *136*, 529-540.

Rospars, J.P., Lansky, P., Chaput, M., and Duchamp-Viret, P. (2008). Competitive and noncompetitive odorant interactions in the early neural coding of odorant mixtures. Journal of Neuroscience *28*, 2659-2666.

Rubin, B.D., and Katz, L.C. (1999). Optical imaging of odorant representations in the mammalian olfactory bulb. Neuron *23*, 499-511.

Saito, H., Kubota, M., Roberts, R.W., Chi, Q.Y., and Matsunami, H. (2004). RTP family members induce functional expression of mammalian odorant receptors. Cell *119*, 679-691.

Sakamoto, M., Ieki, N., Miyoshi, G., Mochimaru, D., Miyachi, H., Imura, T., Yamaguchi, M., Fishell, G., Mori, K., Kageyama, R., *et al.* (2014). Continuous Postnatal Neurogenesis Contributes to Formation of the Olfactory Bulb Neural Circuits and Flexible Olfactory Associative Learning. Journal of Neuroscience *34*, 5788-5799.

Schwartz, T.W., and Holst, B. (2007). Allosteric enhancers, allosteric agonists and ago-allosteric modulators: where do they bind and how do they act? Trends Pharmacol Sci *28*, 366-373.

Shusterman, R., Smear, M.C., Koulakov, A.A., and Rinberg, D. (2011). Precise olfactory responses tile the sniff cycle. Nature neuroscience *14*, 1039-1044.

Stettler, D.D., and Axel, R. (2009). Representations of Odor in the Piriform Cortex. Neuron *63*, 854-864.

Su, C.Y., Menuz, K., Reisert, J., and Carlson, J.R. (2012). Non-synaptic inhibition between grouped neurons in an olfactory circuit. Nature *492*, 66-+.

Tsuboi, A., Imai, T., Kato, H.K., Matsumoto, H., Igarashi, K.M., Suzuki, M., Mori, K., and Sakano, H. (2011). Two highly homologous mouse odorant receptors encoded by tandemly-linked MOR29A and MOR29B genes respond differently to phenyl ethers. The European journal of neuroscience *33*, 205-213.

Wachowiak, M., and Cohen, L.B. (2001). Representation of odorants by receptor neuron input to the mouse olfactory bulb. Neuron *32*, 723-735.

Wachowiak, M., Economo, M.N., Diaz-Quesada, M., Brunert, D., Wesson, D.W., White, J.A., and Rothermel, M. (2013). Optical Dissection of Odor Information Processing In Vivo Using GCaMPs Expressed in Specified Cell Types of the Olfactory Bulb. Journal of Neuroscience *33*, 5285-5300.

Wilson, R.I., and Mainen, Z.F. (2006). Early events in olfactory processing. Annu Rev Neurosci *29*, 163-201.

Xu, L., Li, W., Voleti, V., Hillman, E.M.C., and Firestein, S. (2019). Widespread Receptor Driven Modulation in Peripheral Olfactory Coding. bioRxiv, 760330.

Yokoi, M., Mori, K., and Nakanishi, S. (1995). Refinement of odor molecule tuning by dendrodendritic synaptic inhibition in the olfactory bulb. Proceedings of the National Academy of Sciences of the United States of America *92*, 3371-3375.

Zhang, Y., Tsang, T.K., Bushong, E.A., Chu, L.A., Chiang, A.S., Ellisman, M.H., Reingruber, J., and Su, C.Y. (2019). Asymmetric ephaptic inhibition between compartmentalized olfactory receptor neurons. Nature Communications *10*.

FIGURES

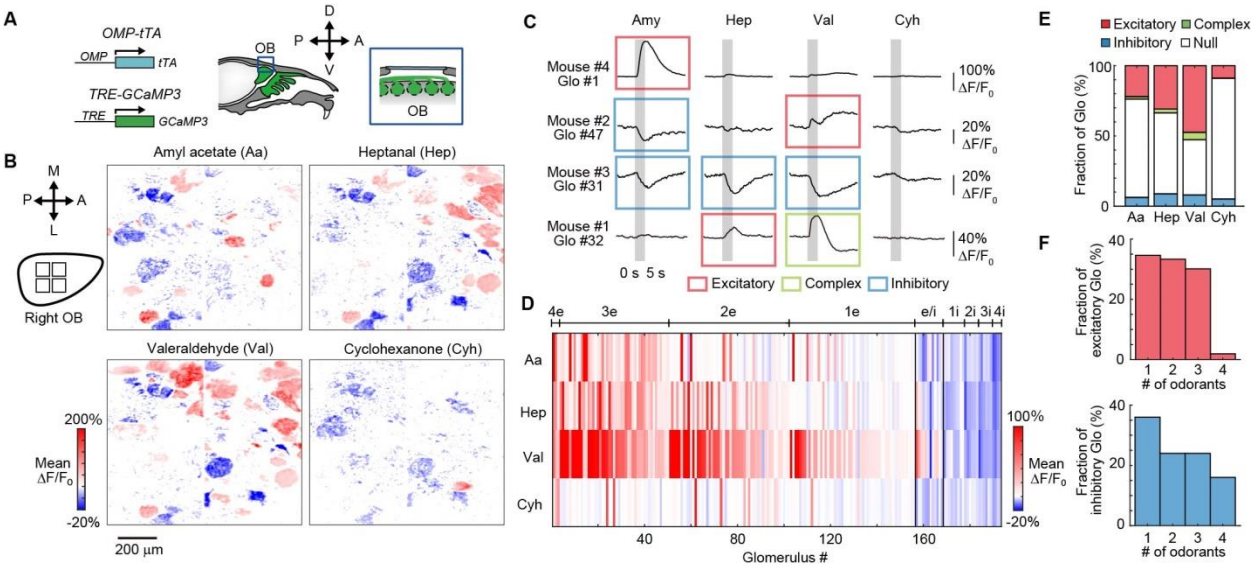

Figure 1. **Odor-evoked inhibitory responses in OSN axons.**

(A) Two-photon calcium imaging of OSN axon terminals *in vivo*. OSN-GCaMP3 mice (OMP-tTA BAC Tg crossed with R26-TRE-GCaMP3 BAC Tg) were used for *in vivo* imaging of OSN axon terminals in the glomerular layer. Only anesthetized mice were analyzed except for Figure S1F, G.

(B) Excitatory (red) and inhibitory (blue) responses at OSN axon terminals in the glomerular layer. Mean $\Delta F/F_0$ per pixel during the first 20 s from the stimulus onset are shown. Scale bar, 200 μm.

(C) Representative glomerular responses at OSN axon terminals to odors (Aa, amyl acetate; Hep, heptanal; Val, valeraldehyde; Cyh, cyclohexanone; diluted at 0.5%). Odors were delivered to the nose for 5 s (shown in gray) under freely breathing conditions.

(D) Glomerular and odor specificity of excitatory and inhibitory responses. Both wide and narrow odor tuning was observed for both excitatory and inhibitory responses. Glomeruli showing responses to at least one odorant were analyzed. Glomeruli are clustered based on the number of excitatory (4e-1e) and inhibitory (1i-3i) odors, and for bidirectional (e/i) responses. Only significant responses (>3 SD above baseline fluctuation) were categorized as excitatory or inhibitory. N = 299 glomeruli from 5 mice. 193 glomeruli showing significant responses to at least one odorant are shown.

(E) Polarity of glomerular responses to each odor. Fractions out of the total number of glomeruli are shown. A small fraction demonstrated complex (excitatory-inhibitory or inhibitory-excitatory) responses.

(F) Tuning specificity of excitatory and inhibitory responses. Data are from 156 and 25 odor-glomerulus pairs for excitatory and inhibitory responses, respectively. Bidirectional glomeruli are not analyzed here.

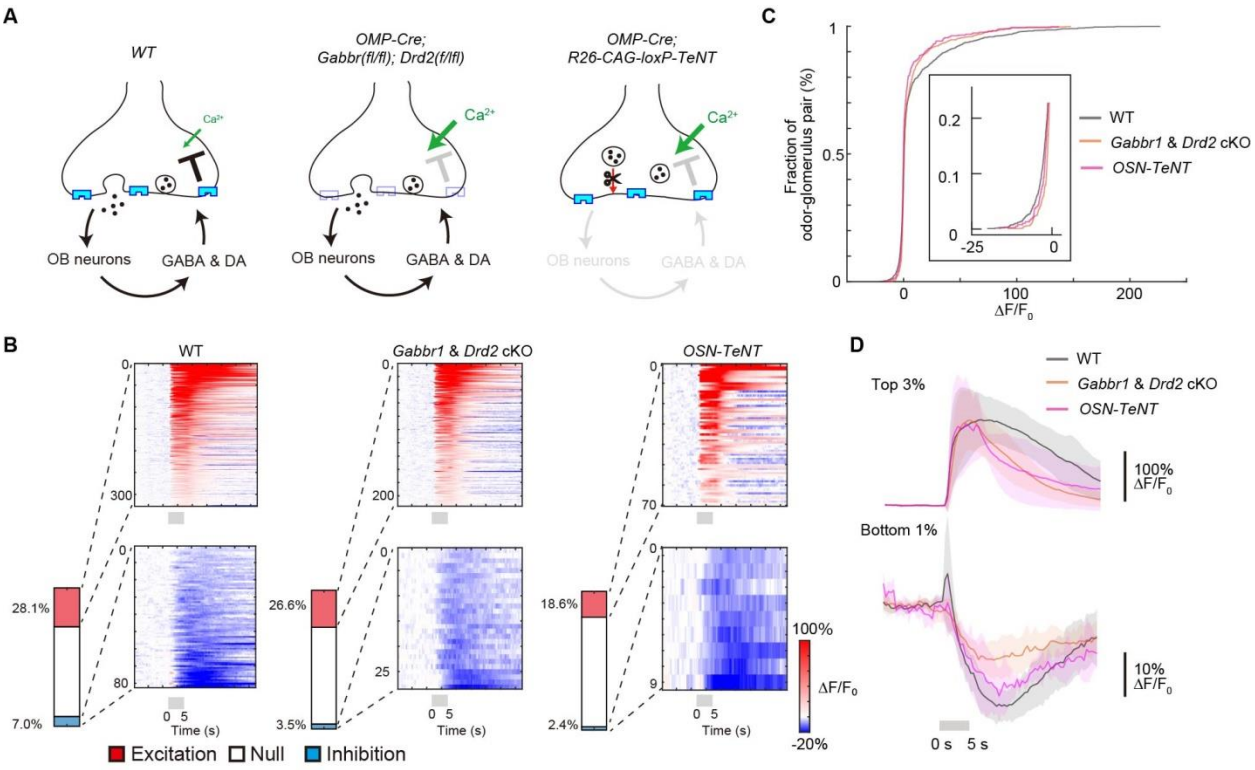

Figure 2. Inhibitory responses at OSN axon terminals without known types of presynaptic inhibition.

(A) Schematic representation of conditional double knockout and OSN-TeNT mutant mice. We generated OSN-specific *Gabbr1* and *Drd2* mutant mice (*OMP-Cre; Gabbr1*$^{fl/fl}$*; Drd2*$^{fl/fl}$) (See Figure S3 for details). OSN axon terminals of *Gabbr1* and *Drd2* cKO mice cannot receive presynaptic inhibition mediated by GABA and DA. We also analyzed OSN-specific TeNT knock-in mice (OSN-TeNT). OSN axons in OSN-TeNT mice cannot release synaptic vesicles (Figure S4), and thus do not receive presynaptic inhibition from OB interneurons.

(B) Excitatory and inhibitory glomerular responses in the mutant mice. Amyl acetate, heptanal, valeraldehyde, and cyclohexanone (diluted at 0.5%) were tested. Stacked barplots indicate the fraction of response polarity in each mouse line (left). Odor-evoked responses across a population of odor-glomerulus pairs sorted by their response amplitude (right). The y-axis represents the odor-glomerulus pairs. WT, N = 1196 odor-glomerulus pairs from 5 mice; *Gabbr1/Drd2* cKO, N = 807 odor-glomerulus pairs from 4 mice; OSN-TeNT, N = 377 odor-glomerulus pairs from 3 mice.

(C) Cumulative histogram of response amplitudes. The inset includes expanded x- and y-axes to display inhibitory response.

(D) Temporal kinetics of excitatory and inhibitory responses. For a fair comparison across genotypes, the top 2% and bottom 1% was used to show the averaged excitatory and inhibitory response kinetics, respectively. WT, N = 34 and 11 odor-glomerulus pairs; *Gabbr1/Drd2* cKO, N = 24 and 8 odor-glomerulus pairs; OSN-TeNT, N = 11 and 3 odor-glomerulus pairs for excitatory and inhibitory responses, respectively. See also Figure S4G.

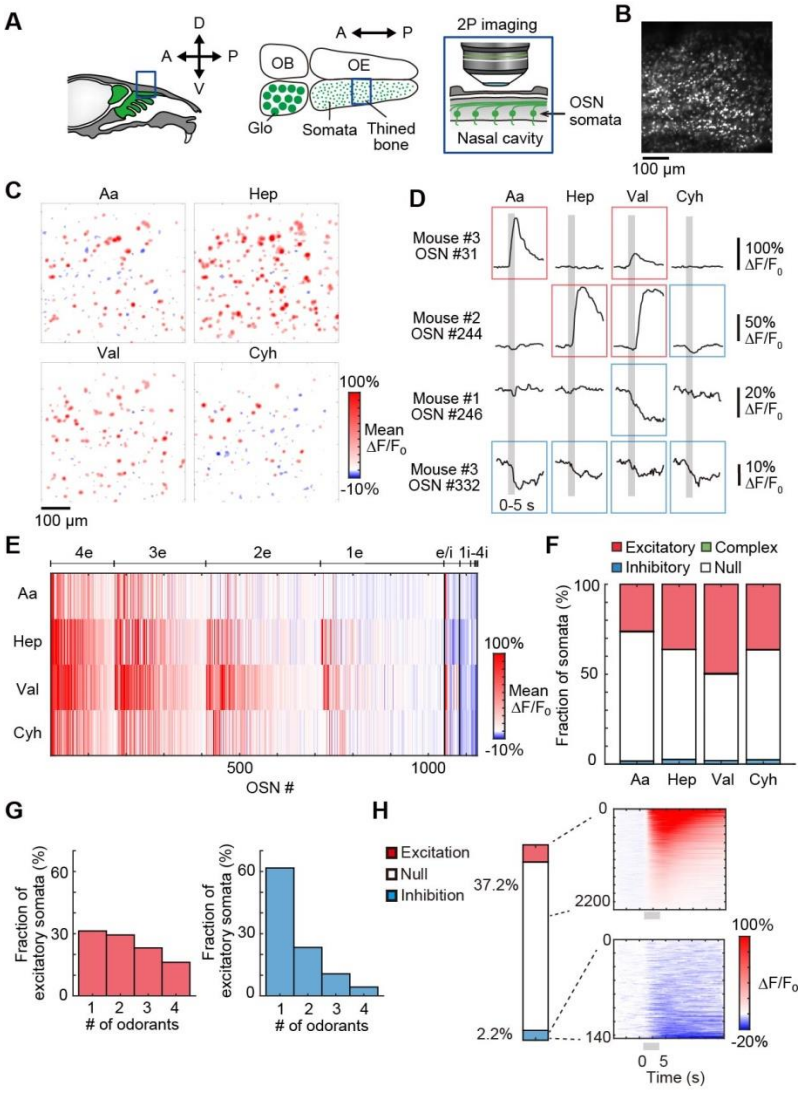

Figure 3. Inhibitory responses at OSN somata in the OE.

(A) Two-photon calcium imaging of OSN somata in the OE *in vivo*. OSNs in the dorsal OE (zone 1) were imaged through thinned nasal bone.

(B) A representative image of basal GCaMP3 fluorescence in the OE. Scale bar, 100 µm.

(C) Widespread inhibitory responses in the OE. Excitatory (red) and inhibitory (blue) responses are shown. Scale bar, 100 µm.

(D) Representative response profiles of OSNs to odors. Odors were delivered to the nose for 5s (shown in gray). Traces for both excitatory and inhibitory responses are shown.

(E) Responsive OSNs are clustered based on the number of excitatory (4e-1e) and inhibitory (1i-3i) odors, and for bidirectional (e/i) responses. Only significant responses (>3SD above baseline fluctuation) were categorized as excitatory or inhibitory. OSNs showing responses to at least one odorant were analyzed. N = 1654 OSNs from 4 mice. 1129 OSNs showing significant responses are shown..

(F) Polarity of odor-evoked responses analyzed for total OSNs. Complex (excitatory-inhibitory or inhibitory-excitatory) responses were not evident in the OE.

(G) Tuning specificity of excitatory and inhibitory responses. Inhibitory responses were more narrowly tuned than in glomeruli. Data are from 1042 and 81 OSNs for excitatory and inhibitory responses, respectively.
(H) Fractions of OSN somata showing excitatory and inhibitory responses. N = 6616 odor-OSN pairs.

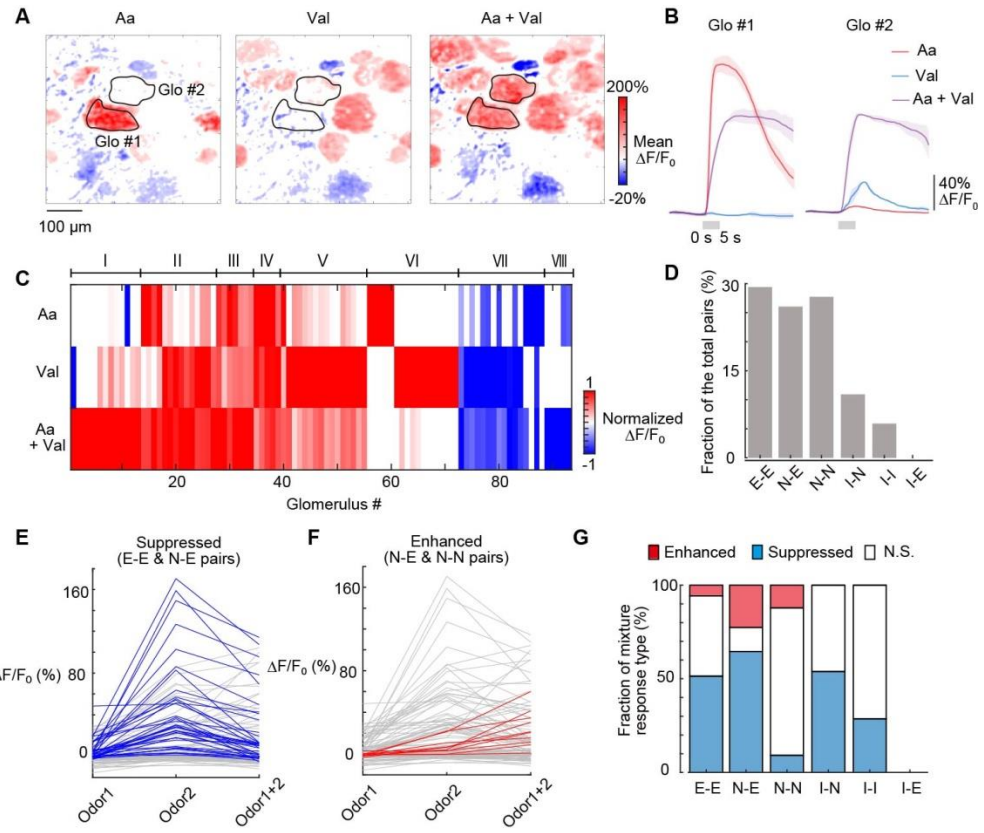

Figure 4. Representation of odor mixtures at OSN axon terminals.

(A) Responses to amyl acetate (Aa), valeraldehyde (Val), and a mixture of them at OSN axon terminals in the glomerular layer. Mean $\Delta F/F_0$ per pixel during the first 20 s from the stimulus onset are shown. Scale bar, 100 μm.

(B) Response profiles of glomerulus #1 and #2 shown in (A). Val suppressed the response of glomerulus #1 to Aa. Aa enhanced the response of glomerulus #2 to Val.

(C) Summary of glomerular responses. Glomeruli are sorted based on the k-means clustering of response profiles. Glomeruli showing responses to at least one odorant are shown. Eight clusters based on k-means clustering are shown (I-VI, mixture responses of excitatory pairs; VII-VIII, mixture responses of inhibitory pairs; I- II, enhancement; III, not significant; IV-V, suppression). N = 131 glomeruli from 3 mice.

(D) Fraction of glomeruli showing excitatory (E), inhibitory (I), or null (N) responses to the two odorants, Aa and Val. Glomeruli were categorized into E-E, N-E, N-N, N-I, I-I, and E-I.

(E) Suppression seen for E-E and N-E glomeruli. Responses to odor 1 (odorant showing the smaller response), odor 2 (the larger response), and the mixture of them are shown. Blue lines indicate glomeruli in which odor 1 suppressed responses to odor 2. All other remaining glomeruli in this category are shown in gray.

(F) Enhanced responses seen for N-E and N-N glomeruli. Responses to odor 1 (smaller response), odor 2 (larger response), and the mixture of them are shown. Red lines indicate glomeruli in which odor 1 non-linearly enhanced responses to odor 2. All other remaining glomeruli in this category are shown in gray.

(G) Fraction of glomeruli demonstrating suppressed and enhanced responses in mixture experiments, shown for each glomerular group.

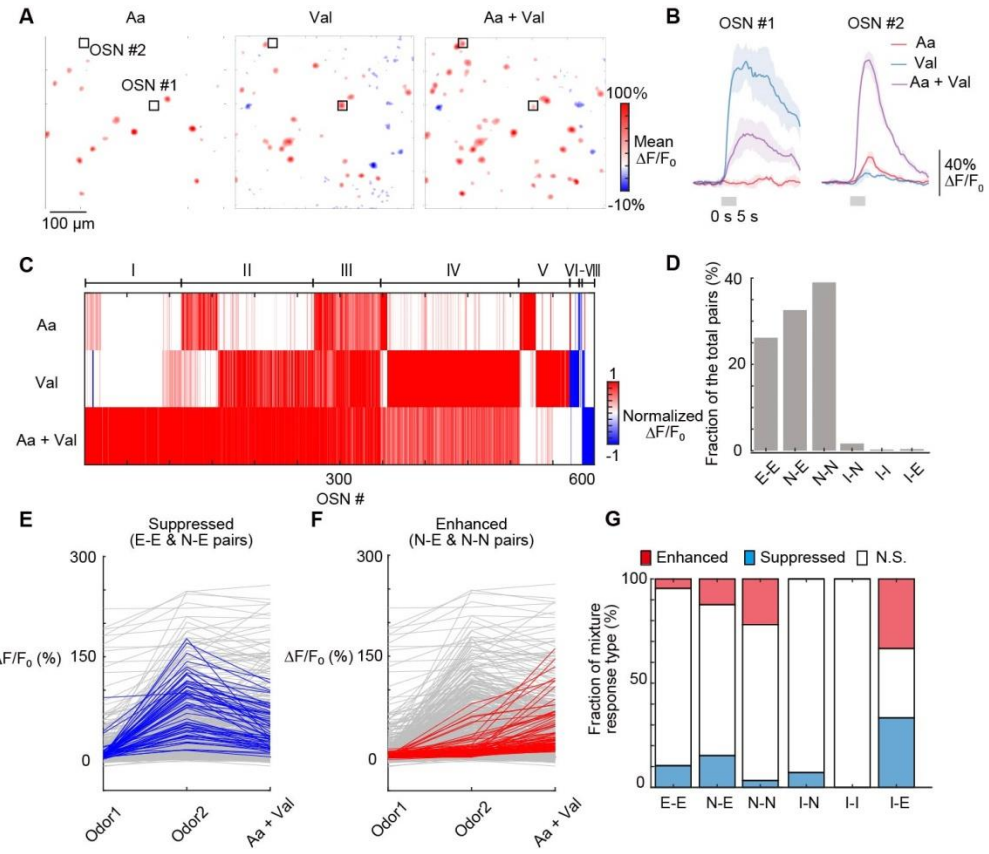

Figure 5. Representation of odor mixtures at OSN somata in the OE.

(A) Responses to amyl acetate (Aa), valeraldehyde (Val), and a mixture of them at OSN somata in the OE. Scale bar, 100 μm.

(B) Response profiles of OSN #1 and #2 shown in (A). Aa suppressed the response of OSN #1 to Val. Val enhanced the response of OSN #2 to Aa.

(C) Summary of OSN responses. Glomeruli are sorted based on the k-means clustering of response profiles. Eight clusters are shown (I-V, mixture responses of excitatory pairs; VI-VIII, mixture responses of inhibitory pairs; I- II, enhancement; III, not significant; IV-V, suppression). N = 862 OSNs from 3 mice.

(D) Fraction of OSNs showing excitatory (E), inhibitory (I), or null (N) responses to the two odorants, Aa and Val. OSNs were categorized into E-E, N-E, N-N, N-I, I-I, and E-I.

(E) Suppressed responses seen for E-E and N-E OSNs. Responses to odor 1 (odorant showing smaller response), odor 2 (larger response), and the mixture of them are shown. Blue lines indicate OSNs in which odor 1 suppressed responses to odor 2. All other remaining OSNs in this category are shown in gray.

(F) Enhanced responses seen for N-E and N-N OSNs. Responses to odor 1 (smaller response), odor 2 (larger response), and the mixture of them are shown. Red lines indicate OSNs in which odor 1 non-linearly enhanced responses to odor 2. All other remaining OSNs in this category are shown in gray.

(G) Fraction of OSNs demonstrating suppression and enhancer effects in mixture experiments, shown for each glomerular group.

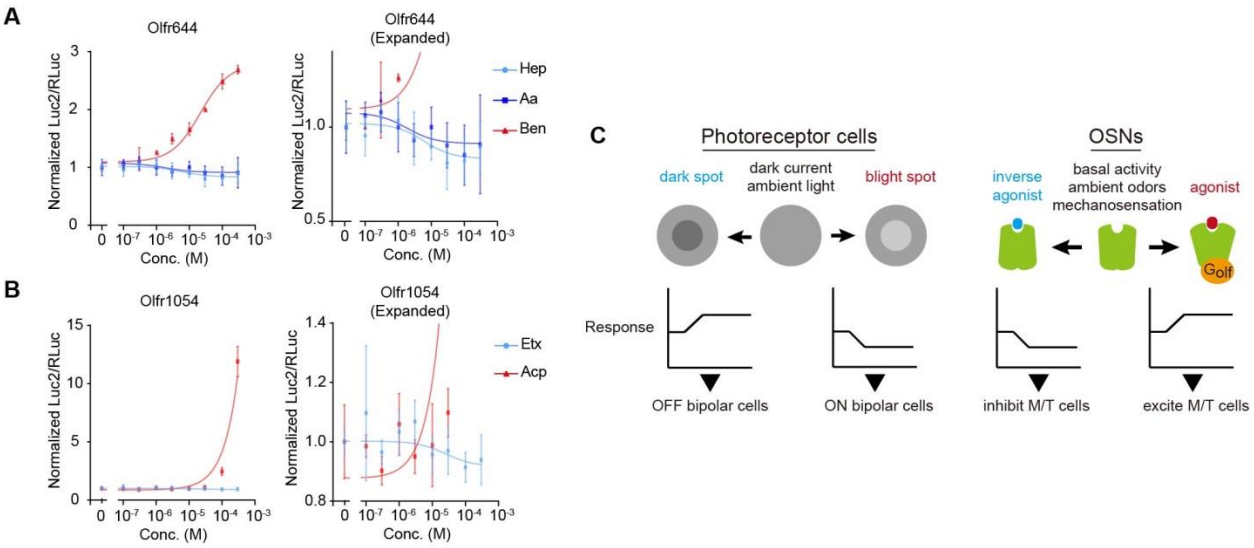

Figure 6. Inhibitory responses in a heterologous assay system for ORs.
(A, B) Dose-response curves of Olfr644 (A) and Olfr1054 (B) for various odorants. ORs were expressed in HEK293 cells with a chaperone molecule, RTP1S. A dual luciferase assay was used to measure cAMP response element (CRE) promoter activity. Benzaldehyde was an agonist for Olf644. However, heptanal and amyl acetate acted as inverse agonists for Olfr644. Similarly, ethylhexanoate acted as an inverse agonist for Olfr1054, whereas acetophenone was an agonist.
(C) Schematic representation of the bidirectional responses in the visual and olfactory systems. In the visual system, dark current and responses to the ambient light set the baseline membrane potential of photoreceptor cells. As a result, photoreceptor cells show bidirectional responses in the physiological conditions, which is useful for detecting bright and dark objects through the ON and OFF pathways. Similarly, in the olfactory system, the basal activity of ORs, ambient odors, and mechanosensation sets the baseline cAMP levels in OSNs. We propose that bidirectional responses are useful for reliable odor identification in noisy sensory environments. This may also be useful for the computation of odor mixtures in the periphery.

METHODS

Mouse strains

All animal experiments were approved by the Institutional Animal Care and Use Committee (IACUC) of the RIKEN Kobe Branch and Kyushu University. BAC transgenic *OMP-tTA* (line #3; Accession No. CDB0506T: http://www2.clst.riken.jp/arg/TG%20mutant%20mice%20list.html) crossed to BAC transgenic *TRE-GCaMP3* mice (high copy line; Accession No. CDB0505T) were described in a previous study (Iwata et al., 2017). *R26-CAG-LoxP-TeNT* knock-in (RBRC05154)(Sakamoto et al., 2014), *OMP-Cre* knock-in (JAX #006668)(Li et al., 2004), and *Thy1-GCaMP6f* Tg (line GP5.11) (JAX #024339)(Dana et al., 2014) have been described previously. $Drd2^{tm1a}$ and $Gabbr1^{tm1a}$ mice were produced from ES clones obtained from EUCOMM and KOMP, respectively. Among the three clones each for $Drd2^{tm1a}$ and $Gabbr1^{tm1a}$, only $Drd2^{tm1a(EUCOMM)Hmgu}$ (HEPD0654_5_D11) and $Gabbr1^{tm1a(KOMP)Wtsi}$ (EPD0730_1_G04) were transmitted to the germ line. Southern blotting was used to confirm correct gene targeting. These mice were then crossed to *Flp* mice (JAX# 003800) to delete *lacZ-Neo*^{r} cassette and obtain $Drd2^{tm1c}$ and $Gabbr1^{tm1c}$ (Figure S3). Genotyping primers were 5'-TCACCCTCCAGCCTGCCTAC-3' and 5'-CGTCGCGATGTGAGAGGAGA-3' for *OMP-tTA* mice; 5'-AACCGTCAGATCGCCTGGAG-3' and 5'-CGGTACCGCCCTTGTACAGC-3' for *TRE-GCaMP3* mice; 5'-TGTGGAAGGCAATTCTGAGAGG-3' and 5'- CCACTTTGTACAAGAAAGCTGGGTCT-3' for $Gabbr1^{tm1c}$ allele; 5'- GTTGCCTTCCCCCTCTTGCT-3' and 5'-CCACTTTGTACAAGAAAGCTGGGTCT-3' for $Drd2^{tm1c}$ allele (the primer sites are indicated in Figure S3). *OMP-Cre* was in a 129/C57BL/6 mixed background and all other lines were in a C57BL/6N background. Both male and female mice were used.

Southern blotting

Genomic DNA (10 μg) extracted from the mouse tail was digested with restriction enzymes: *KpnI* (Toyobo), *ApaI* (NEB, R0114S), *SpeI* (NEB, R0133S), and *XhoI* (NEB, R0146S). Electrophoresed agarose gels were treated with 0.4% (v/v) HCl and then alkaline transferred with 0.4 M NaOH to Biodyne Plus Membrane (0.45 μm, Pall Corporation, #60406). Hybridization with DIG-labelled DNA probes was performed in Church's buffer at 65°C overnight. Blocking was performed with 1.5% Blocking Reagent (Roche, #11096176001), and 0.1% Anti-Digoxigenin-AP Fab fragments (Roche, #11093274910) in blocking buffer was used to detect DIG. Chemiluminescence reaction was performed with CDP-Star substrate (Thermo Fisher, #11685627001), and detected with an image reader (Fujifilm, LAS-3000 mini). DNA Probes were labelled with DIG-High prime (Roche, #1585606). The locations of DNA probes are indicated in Figure S3. Primer sequences for the probes are 5'-GGAAACTGGGAGGTGGCTCA-3' and 5'-ATCAGGCTTGGCTTGGCTTG-3' for *Drd2* upstream; 5'-CTGGGGAGACCACCAGCAGT-3' and 5'-CATGGATCCAACCCCAGAGC-3' for *Drd2* downstream; 5'-GTCAGTTCTTGGCCGCAAGC-3' and 5'-

ACTTTCCGGGCTTCGGTCTC-3' for *Gabbr1* upstream; 5'-TCCTGCAGTTCCATCCACCA-3' and 5'-CCACCCGAGTTTTGGGATTG-3' for *Gabbr1* downstream; 5'-GCGATACCGTAAAGCACGAG-3' and 5'-GCTTGGGTGGAGAGGCTATT -3' for *Neo*^{r} probe.

Histochemistry

Mice were deeply anesthetized with an overdose i.p. injection of pentobarbital. After intracardiac perfusion with 4% PFA in PBS, the OB was dissected and post-fixed in 4% PFA in PBS overnight. The OB was then cryoprotected with 30% sucrose, and then embedded in OCT Compound (Sakura). Frozen sections were cut at 18μm thick with a cryostat (Leica). Antigen retrieval was performed by heating in a microwave oven for 5 min in Histofine antigen retrieval solution pH9 (Nichirei, #415201). Sections were pretreated with 4% PFA in PBS, and 5% Donkey serum (Jackson) in PBS with 0.1% Triton-X100. Rabbit anti-Drd2 (Millipore, AB5084P) and guinea pig anti-Gabbr1 (Millipore, AB2256) were used at 1:100 and 1:500 dilutions, respectively. AlexaFluor647-conjugated secondary antibodies (Life technologies, A31573 and A21450) were used at 1:200 dilutions. Sections were counterstained with DAPI (Dojindo). Immunofluorescence was imaged with an inverted confocal laser-scanning microscope (Olympus, FV1000) using a 20x dry objective lens (Olympus).

***In vivo* two-photon imaging**

In vivo imaging of the OB and OE was performed as described previously (Iwata et al., 2017). Adult mice (8-16 weeks of age) were used for imaging. Surgery and imaging under anesthesia was performed under ketamine/xylazine (80 mg/kg and 16 mg/kg, respectively) anesthesia. During surgery and imaging, the depth of anesthesia was assessed by the toe-pinch reflexes, and supplemental doses were added when necessary. For the imaging of the OB, a craniotomy (2-3 mm in diameter) was made over the dorsal OB leaving the dura mater intact. The OB was covered with a thin layer of silicone sealant (Kwik-Sil, WPI) and a 3 mm diameter circular coverslip (Matsunami), which was secured with super-glue and dental cement (Shofu). For the imaging of the OE, the dorsal part of the D zone (zone 1) OE was imaged through the thinned nasal bone. We used a dental drill with a 1mm drill tip to evenly thin the nasal bone. PBS was applied to the thinned area during the imaging. For head-fixation, a custom aluminum head bar (4 × 22 mm) was glued to the skull behind the cranial window. Body temperature was maintained with a heating pad (Akizuki, M-08908). In some experiments (Figure S1F, G), we imaged awake mice as described previously (Guo et al., 2014; Iwata et al., 2017). Water-restriction was started 2-3 days after surgery. Mice under water-restriction were acclimated to head-fixation in an acrylic tube within 3-4 days, 30 min each. Mice were kept in the acrylic tube during the imaging. Imaging with artificial sniffing was performed as described previously (Iwata et al., 2017). The silicon tube inserted into trachea was connected to a solenoid valve, a flow meter, and an air suction pump in all the experiments. The solenoid valves for nasal airflow

and odor delivery were regulated through relay circuits and the computer programs were written in LabVIEW (National Instruments).

Olfactometry

Olfactory stimulation using olfactometer was described previously (Iwata et al., 2017). The olfactometer consists of an air pump (AS ONE, #1-7482-11), activated charcoal filter (Advantec, TCC-A1-S0C0 and 1TS-B), and flowmeters (Kofloc, RK-1250). Odorants were diluted at 0.5% in 1 mL of mineral oil in a 50mL centrifuge tube. Saturated odor vapor in the centrifuge tube was delivered to a mouse nose with a Teflon tube. The tip of the Teflon tube was located 1 cm from the nose of animals. Diluted odors were delivered at 1 L/min. Odorants (amyl acetate, heptanal, valeraldehyde, and cycrohexanoate) were purchased from Tokyo Kasei (cat# A0021, C0489, V0001, H0025), stored at 4 $^{\circ}$C, and diluted in mineral oil just prior to use. 50 mL centrifuge tubes and Teflon tubes were replaced to new one every time we change odors.

Image data analysis

All image data analysis was performed in MATLAB (Mathworks). Lateral drift in time-lapse imaging data was corrected using custom code based on correlation coefficient. ROIs for glomeruli and somata were manually determined. The ΔF was normalized to the mean intensity for 10 s before stimulus onset (F_0), and the response amplitude was defined as the mean $\Delta F/F_0$ during the first 20 s after stimulus onset. When the mean $\Delta F/F_0$ was higher or lower than 3SD of basal fluctuation level before stimulation onset, the response was categorized as excitatory or inhibitory, respectively. Some glomeruli or OSNs demonstrated tonic increase or decrease of GCaMP fluorescence before odor stimulation. We therefore excluded data when a response slope (0-3 s after the stimulus onset) of a glomerulus/OSN was within 50-150% of that before stimulus onset. To detect complex responses, the mean $\Delta F/F_0$ during the 0-10 s and 10-20 s after stimulation onset were compared to $F_0 \pm 3$SD of basal fluctuation level before stimulation onset, respectively. If one of them showed significantly higher value and another showed lower value, the responses were categorized as complex responses. Temporal median filtering with 3 s window size was applied to the data of OSN somata to make its noise fluctuation level similar to those of glomeruli. To determine the antagonistic effects in odor mixture experiments, we performed two-tailed t-test with Odor2 (one of the two odorants, evoking higher response than the other) and Odor1+2. As for the enhancer effects in mixture experiments, we compared linear summation of Odor1 and Odor2 responses versus Odor1+2 response. Codes are available upon request.

Luciferase assay

Luciferase assay with HEK 293 cells (293AAV cell, Cell Biolabs) was performed as described previously (Tsuboi et al., 2011). ORs and *Rtp1* (coding for RTP1S) genes were PCR amplified

from cDNA prepared from C57BL6/N mouse OE and subcloned into pME18S-F-R vector and pcDNA3, respectively. In pME18S-F-R vector, OR genes are expressed under SRα promoter. OR has N-terminal FLAG-tag and 20aa rhodopsin tag to facilitate cell surface expression. Cells were grown in DMEM supplemented with 10% FBS and 1% Penicillin/Streptomycin. Cells seeded in 96-well white-well plates (60% confluent) were transfected with pME18S-F-R-OR (125 ng/well), CRE-Luc2P (25 ng/well; Promega pGL4.29), TK-hRluc (25 ng/well, Promega pGL4.74) and pcDNA3-RTP1s (25 ng/well) using PEI Max (Polysciences, Inc.). Twenty-four hours after the transfection, the medium was replaced with DMEM with odor ligands and without serum. To avoid contamination of odors to other wells, wells were separated at least 3 wells from the ones containing different stimulation medium and sealed with a plastic film, SealPlate (Excel Scientific, #STRSEALPLT), during incubation. Cells were incubated for 4 hrs, and then Luc2P and hRluc activities were quantified with Dual-Glo Luciferase assay system (Promega, #E2920) and a luminometer, model TriStar LB941 (Berthold). Data are mean ± SD based on 3 and 6 replicates for agonist and inverse-agonist in one representative experiment, respectively. Hill curve fitting was applied to the dose-response data by using Prism software (GraphPad Software). Reproducibility was confirmed by multiple experiments. Newly generated pME18S-F-R-OR plasmids will be deposited to Addgene. To identify inverse agonists, we have analyzed 85 ORs. In the initial screen, we identified 11 ORs showing the highest basal activity without odorants. We then analyzed responses to 9 odorants (amyl acetate, acetophenone, benzaldehyde, cyclohexanone, ethylhexanoate, heptanal, hexanoic acid, valeraldehyde, and methyl valerate at 300 μM). Agonists and inverse agonists were further analyzed for dose-response curves.

Statistical analysis

MATLAB Statistics Toolbox was used for statistical analysis. Number of glomeruli, cells and mice was described within figure legends. No blinding was performed in data analysis. Two-tailed Student t-test was used in Figure 4 and 5. Statistical significance was set at $P < 0.05$. We did not perform data exclusion.

DATA AND SOFTWARE AVAILABILITY

Newly generated plasmids will be deposited to Addgene. Requests for additional data should be directed to and will be fulfilled on reasonable request by the Lead Contact, Takeshi Imai (t-imai@med.kyushu-u.ac.jp).

SUPPLEMENTAL FIGURES

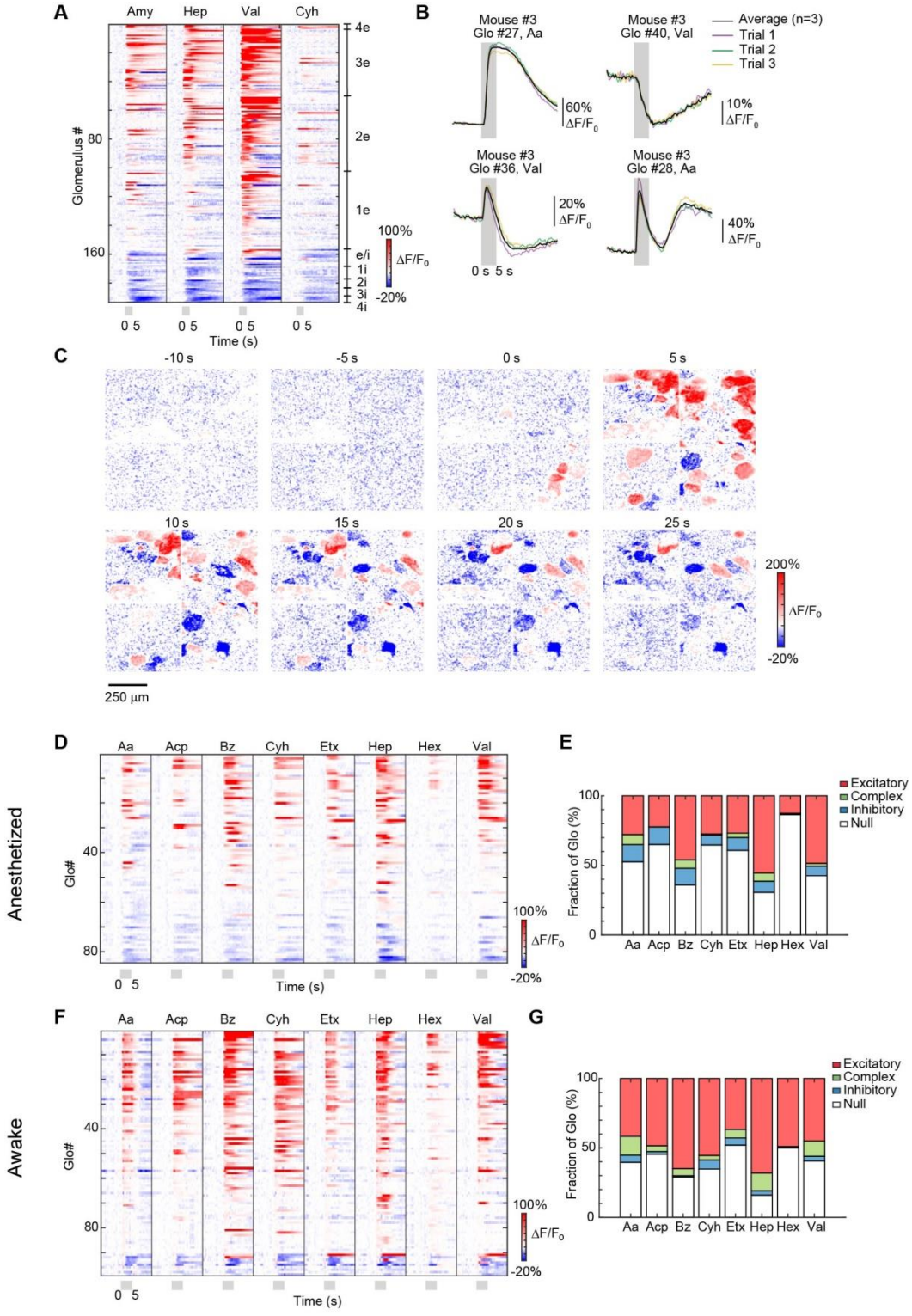

Figure S1. Inhibitory responses at OSN axon terminals.
(A) Temporal profiles of odor-evoked responses at OSN axon terminals. The responses were

sorted based on the number of odorants that elicited odor-evoked responses and their amplitudes. Inhibition was commonly found among different odorants. N = 299 glomeruli from 5 mice. 193 glomeruli showing significant responses to at least one odorant are shown.
(B) Reproducibility of odor-evoked excitatory and inhibitory responses (N = 3 trials each). The glomeruli showed consistent responses to repeated stimuli.
(C) Spatiotemporal profiles of odor (Val) -evoked excitatory and inhibitory responses at OSN axon terminals in the glomerular layer. Scale bar, 250 μm.
(D-G) Widespread inhibitory responses in both anesthetized (D, E) and awake (F, G) animals (N = 3). Larger responses seen in awake mice may be due to the higher sniffing speed/rate. Temporal profiles (D, F) and polarity of odor-evoked responses (E, G) in all glomeruli are shown. N = 105 glomeruli from 5 mice. 84 and 99 glomeruli showing significant responses to at least one odorant are shown for anesthetized and awake state, respectively.

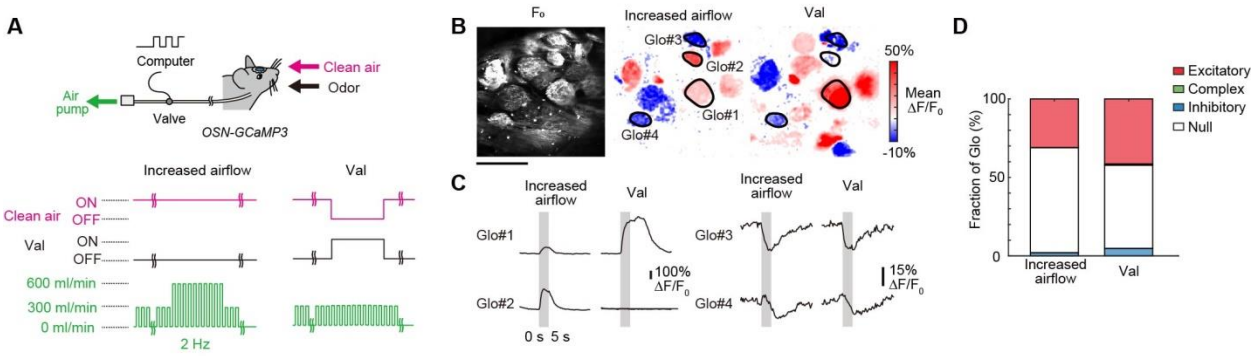

Figure S2. Inhibitory responses by airflow stimulation.

(A) Artificial sniffing system to examine the mechanosensation (left, Increased airflow) and odor responses (right, Val) in tracheotomized and anesthetized mice. Increased airflow or Val stimulation was applied during artificial sniffing (bellow). The timing of airflow generation was controlled by the opening of electromagnetic valves.

(B) Excitatory and inhibitory responses seen for increased airflow (center) and Val stimuli (right). Excitatory and inhibitory responses are shown in red and blue, respectively. Scale bar, 200 μm.

(C) Representative mechanosensory responses to increased airflow and Val-evoked responses. Pulsed airflow (2Hz, 250 ms on and 250 ms off) was artificially produced during the imaging session. Increased airflow (300 to 600 mL/min) or Val stimulation was delivered to the same animal for 5 s (shown in gray).

(D) Fraction of glomeruli showing excitatory and inhibitory responses to increased airflow and Val stimuli. N = 149 glomeruli from 3 mice.

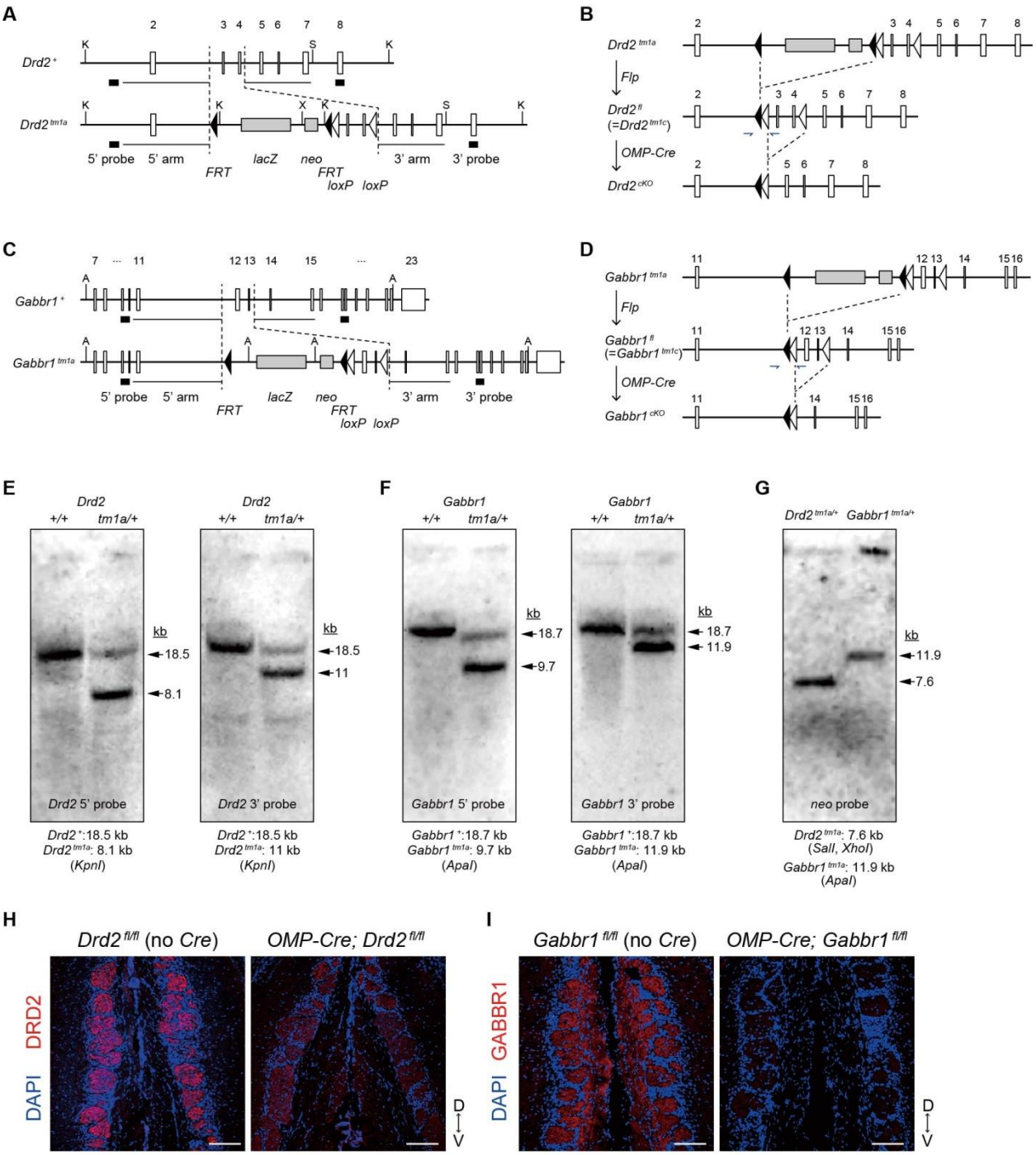

Figure S3. OSN-specific GABAR$_{B1}$ and D2R knockout mice and OSN-specific TeNT knock-in mice.

(A) Gene targeting at *Drd2* locus. We obtained germline transmission from one ES clone, HEPD064_5_D11.

(B) The *Drd2* locus in *Drd2*^{tm1a}, *Drd2*^{fl} (= *Drd*^{tm1c}) and *Drd*^{cKO}. *Drd2*$^{+/tm1a}$ mice were crossed with Flp mice to obtain *Drd2*$^{+/fl}$.

(C) Gene targeting at *Gabbr1* locus. We obtained germline transmission from one ES clone, EPD0730_1_G04.

(D) The *Gabbr1* locus in *Gabbr1*^{tm1a}, *Gabbr1*^{fl} (=*Gabbr1*^{tm1c}), and *Gabbr1*^{cKO}. *Gabbr1*$^{+/tm1a}$ mice were crossed with *Flp* mice to obtain *Gabbr1*$^{+/fl}$.
(E-G) Southern blot analysis on *Drd2*$^{+/+}$ and *Drd2*$^{tm1a/+}$ (E, *Drd2* probe), *Gabbr2*$^{+/+}$ and *Gabbr2*$^{tm1a/+}$ (F, *Gabbr1* probe); *Drd2*$^{tm1a/+}$ and *Gabbr1*$^{tm1a/+}$ (G, *neo*^{r} probe).
(H) Immunostaining of D2R in the OB of OSN-specific *Drd2* mutant mice.
(I) Immunostaining of $GABAR_{B1}$ in the OB of OSN-specific *Gabbr1* mutant mice.
Location of 5' and 3' arms for gene targeting, and 5' and 3' DNA probes for southern blotting are shown in (A) and (C). *KpnI* (K), *SpeI* (S), *XhoI* (X) and *ApaI* (A).

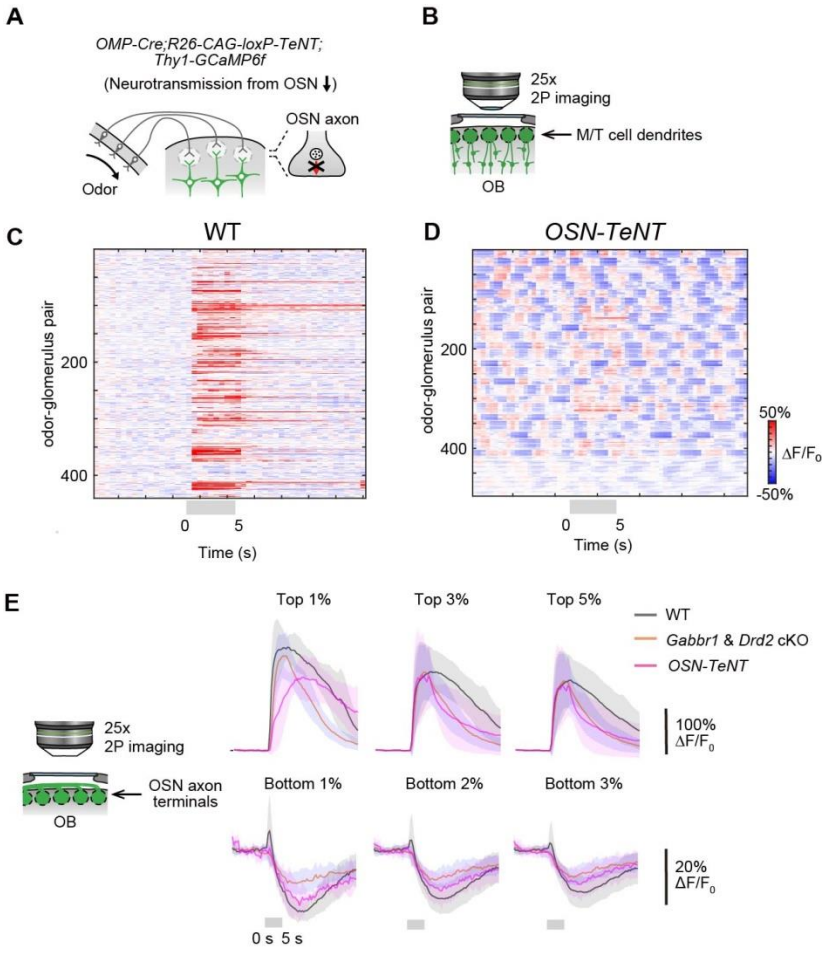

Figure S4. OSN-specific TeNT knock-in mice.
(A) *OMP-Cre* knock-in mice were crossed with *R26-CAG-loxP-TeNT* knock-in mice to obtain OSN-specific TeNT knock-in mice (OSN-TeNT). VAMP2 staining was eliminated at OSN axon terminals in this mouse (Fujimoto et al., 2019).
(B) *Thy1-GCaMP6f* mouse line was used to examine the odor responses in OSN-TeNT mice. (C, D) Odor-evoked responses of M/T cells in wild-type (C) and OSN-TeNT mice (D). Summary of odor-evoked responses in total glomeruli are shown. Odor-evoked responses were almost completely abolished in OSN-TeNT mice. Instead, the M/T cells demonstrated synchronized and oscillatory spontaneous activity (D). N = 440 odor-glomerulus pairs (55 glomeruli) from 3 mice; OSN-TeNT, N = 496 odor-glomerulus pairs (62 glomeruli) from 3 mice. Tested odorants are: amyl acetate, acetophenone, benzaldehyde, cyclohexanone, ethyl hexanoate, heptanal, hexanoic acid, and valeraldehyde, diluted at 0.5%.
(G, H) Temporal kinetics of excitatory (G) and inhibitory responses (H) of OSN axon terminals averaged across different fraction of odor-glomerulus pairs. For fair comparison across mutant lines, the top (1, 3 and 5%) and bottom (1, 2 and 3%) fractions were used to show averaged excitatory and inhibitory response kinetics, respectively.

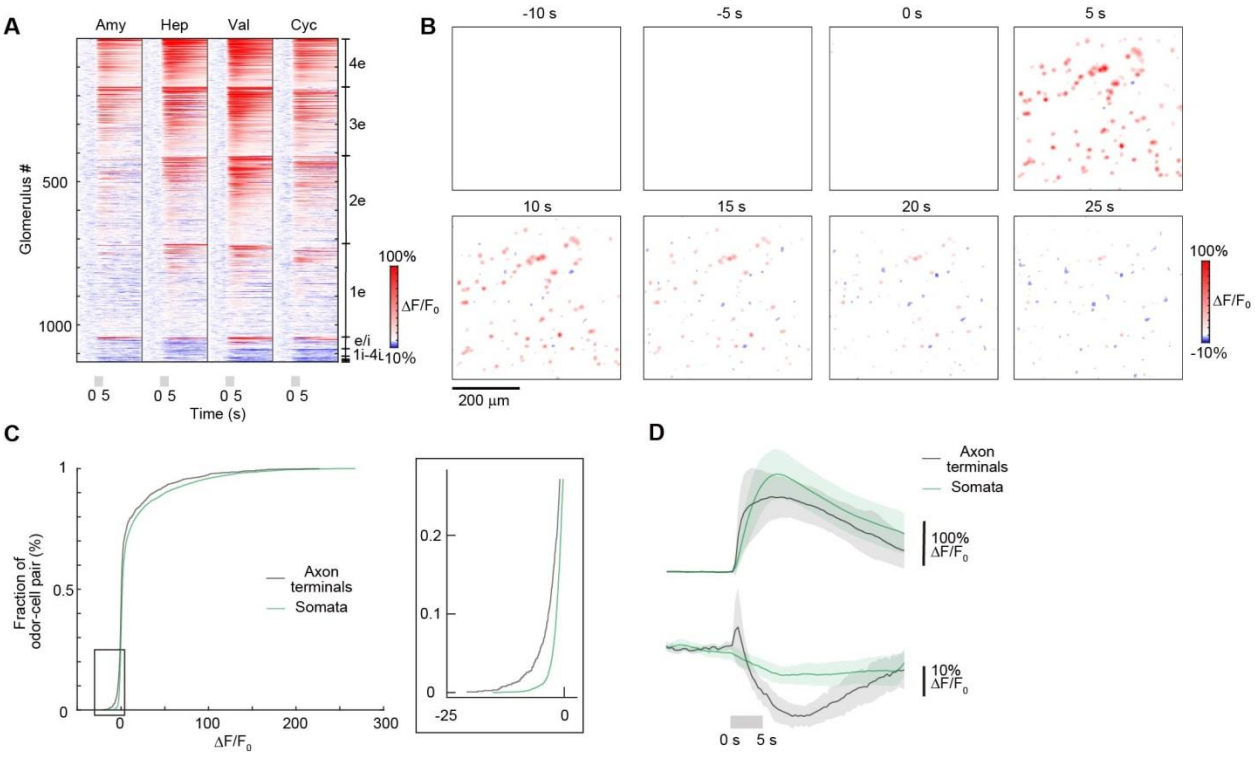

Figure S5. Inhibitory responses in the OSN somata in the OE.

(A) Temporal profiles of odor-evoked responses in OSN somata. The responses were sorted by the number of odorants that elicit odor-evoked responses and their amplitude. Inhibition was commonly found for all four odors. N = 1654 OSNs from 4 mice. 976 OSNs showing significant responses to at least one odorant are shown.

(B) Spatiotemporal profiles of odor (Val) -evoked excitatory (red) and inhibitory (blue) responses in the OSN somata in the OE. Scale bar, 200 μm.

(C) Comparison of OSN axon terminals vs OSN somata. Cumulative histogram of response amplitude for axon terminals and somata. Inset includes expanded *x*- and *y*-axes to display the population showing inhibitory responses. N = 1192 odor-glomerulus pairs from 5 mice for axon terminals; N = 6616 odor-OSN pairs from 4 mice for somata.

(D) Temporal kinetics of excitatory and inhibitory responses in OSN somata and axon terminals. For fair comparisons, the top 3% and bottom 1% were averaged for excitatory and inhibitory traces, respectively. Data are from 35 and 11 odor-glomerulus pairs for excitatory and inhibitory responses, respectively, at axon terminals; Data are from 198 and 66 odor-OSN pairs for somata.

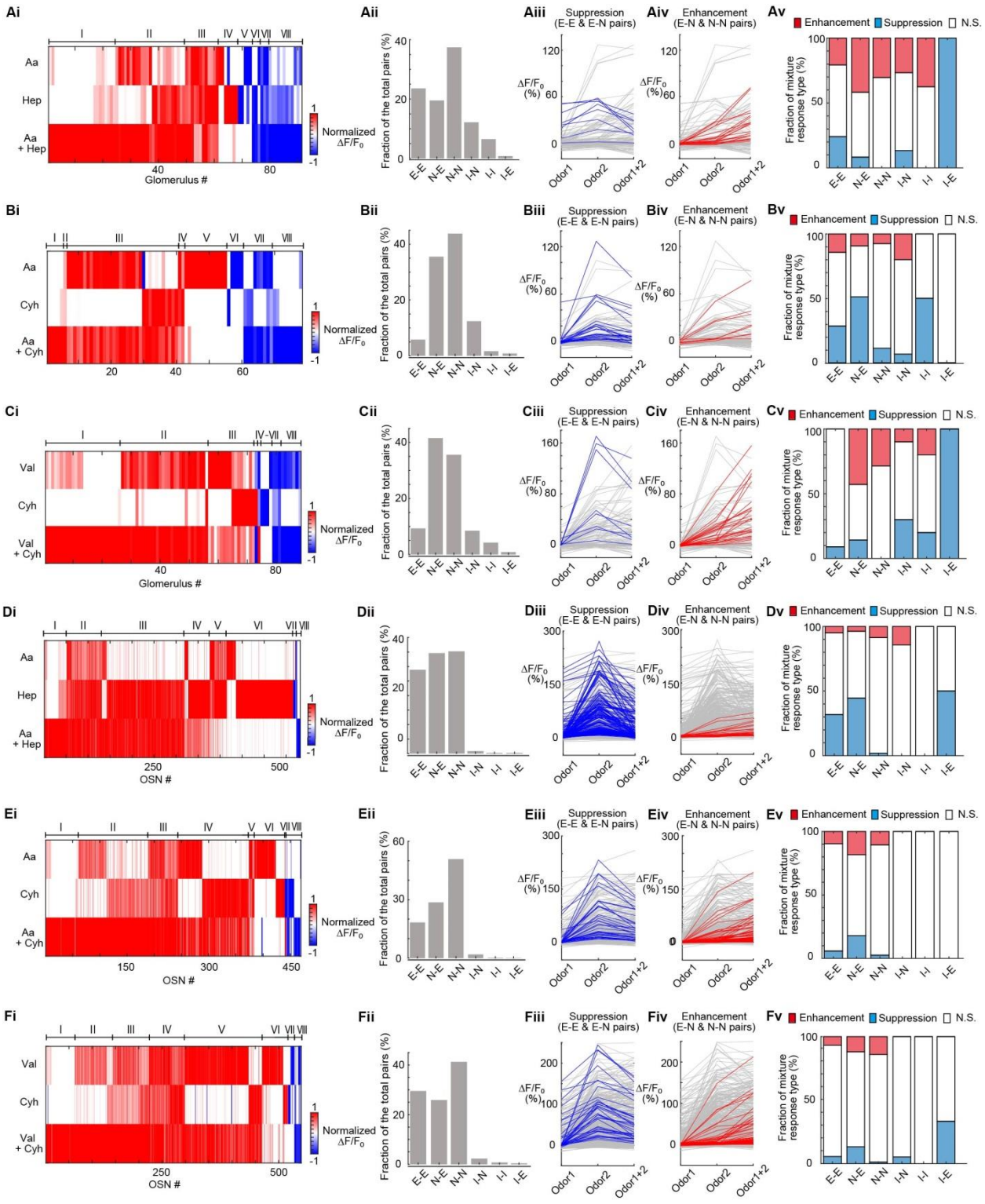

Figure S6. Representation of odor mixtures at OSN axon terminals and somata.
Summary of OSN axon terminals (A-C) and somata (D-F) responses in different odor mixture pairs (A, D: Aa vs Hep; B, E: Aa vs Cyh; C, F: Val vs Cyh) are shown. N = 131 glomeruli from 3 mice; N = 862 OSNs from 3 mice. Data are shown for 91 (A), 789 (B), and 88 (C) glomeruli

for OSN axon terminals; N = 581 (D), 469 (E) and 548 (F) OSNs for somata, showing significant responses to at least one condition.
(i) Summary of OSN responses. Glomeruli or somata are sorted based on the k-means clustering of response profiles. Eight clusters are shown.
(ii) Fraction of glomeruli/OSNs showing excitatory (E), inhibitory (I), or null (N) responses to the two odorants. OSNs were categorized into E-E, N-E, N-N, N-I, I-I, and E-I.
(iii) Antagonism seen for E-E and N-E glomeruli/OSNs. Responses to odor 1 (odorant showing smaller response), odor 2 (larger response), and the mixture of them are shown. Blue lines indicate glomeruli/OSNs in which odor 1 inhibited responses to odor 2. All other remaining glomeruli/OSNs in this category are shown in gray.
(iv) Enhancer effects seen for N-E and N-N categories. Responses to odor 1 (smaller response), odor 2 (larger response), and the mixture of them are shown. Red lines indicate OSNs in which odor 1 non-linearly enhanced responses to odor 2. All other remaining OSNs in this category are shown in gray.
(v) Fraction of OSNs demonstrating antagonism and enhancer effects in mixture experiments, shown for each glomerular group.